Biochimica et Biophysica Acta 1797 (2010) 494–500

Contents lists available at ScienceDirect

Biochimica et Biophysica Acta

journal homepage: www.elsevier.com/locate/bbabio

X-ray absorption studies of Zn^{2+}-binding sites in *Escherichia coli* transhydrogenase and its βH91K mutant

Giulia Veronesi [a,b,1], Simon J. Whitehead [c,1], Francesco Francia [d], Lisa Giachini [e], Federico Boscherini [a,b], Giovanni Venturoli [d,f], Nick P.J. Cotton [c], J. Baz Jackson [c,*]

[a] *Dipartimento di Fisica, Università di Bologna, viale C. Berti Pichat 6/2, 40127, Bologna, Italy*
[b] *OGG-INFM-CNR, c/o ESRF, BP220, F-38043 Grenoble, France*
[c] *School of Biosciences, University of Birmingham, Edgbaston, Birmingham, B15 2TT, UK*
[d] *Laboratorio di Biochimica e Biofisica, Dipartimento di Biologia, Università di Bologna, via Irnerio 42, 40126 Bologna, Italy*
[e] *Australian Synchrotron, 800 Blackburn Rd, Clayton, Victoria 3168, Australia*
[f] *CNISM, c/o Dipartimento di Fisica, Università di Bologna, viale C. Berti Pichat 6/2, 40127, Bologna, Italy*

ARTICLE INFO

Article history:
Received 9 November 2009
Received in revised form 8 January 2010
Accepted 11 January 2010
Available online 18 January 2010

Keywords:
Transhydrogenase
XAFS
Zinc-binding site
Metal-ion inhibition
Proton translocation

ABSTRACT

Transhydrogenase couples hydride transfer between NADH and $NADP^+$ to proton translocation across a membrane. The binding of Zn^{2+} to the enzyme was shown previously to inhibit steps associated with proton transfer. Using Zn K-edge X-ray absorption fine structure (XAFS), we report here on the local structure of Zn^{2+} bound to *Escherichia coli* transhydrogenase. Experiments were performed on wild-type enzyme and a mutant in which βHis91 was replaced by Lys (βH91K). This well-conserved His residue, located in the membrane-spanning domain of the protein, has been suggested to function in proton transfer, and to act as a ligand of the inhibitory Zn^{2+}. The XAFS analysis has identified a Zn^{2+}-binding cluster formed by one Cys, two His, and one Asp/Glu residue, arranged in a tetrahedral geometry. The structure of the site is consistent with the notion that Zn^{2+} inhibits proton translocation by competing with H^+ binding to the His residues. The same cluster of residues with very similar bond lengths best fits the spectra of wild-type transhydrogenase and βH91K. Evidently, βHis91 is not directly involved in Zn^{2+} binding. The locus of βHis91 and that of the Zn-binding site, although both on (or close to) the proton-transfer pathway of transhydrogenase, are spatially separate.

1. Introduction

Divalent metal ions, such as Zn^{2+} and Cd^{2+}, inhibit the catalytic cycle of a number of important membrane proteins, including the cytochrome bc_1 complex [1] cytochrome oxidase [2,3], and the bacterial photosynthetic reaction center [4]. There is evidence that in each case the metal ions block proton-transfer steps. In photosynthetic reaction centers the metal-ion binding site was located at the cytoplasmic surface of the protein by X-ray crystallography. The Zn^{2+}-ligand cluster is formed by the imidazole side chains of two His residues, by the side chain of an Asp, and most likely by a water molecule [5]. The tetrahedral coordination geometry was subsequently confirmed by X-ray absorption fine structure (XAFS), which allowed a high-resolution determination of the bond lengths [6]. Cd^{2+} can also bind at this site but in an octahedral geometry by a cluster which involves the same amino acid residues and possibly four water molecules [7]. The X-ray crystallography and XAFS data provide detailed structure information on the mechanism by which Zn^{2+} and Cd^{2+} obstruct proton entry into the reaction center protein [4–7]. Biochemical studies indicate that a similar mechanism may be relevant to metal-ion inhibition of other H^+-translocating redox complexes [1–3,8]. Structural information on the high-affinity Zn^{2+}-binding sites of cytochrome bc_1 complex [9,10] and of cytochrome *c* oxidase [11,12] are consistent with the proposed inhibition mechanism, and indicate that at least one His residue is always present in the metal binding cluster.

Low concentrations of Zn^{2+}, Cd^{2+} and other metal ions were recently shown to inhibit specific catalytic steps in transhydrogenase [13,14]. This enzyme, found in the inner mitochondrial membrane of animal cells and in the cytoplasmic membrane of many bacteria, couples a redox reaction, hydride transfer between NAD(H) and NADP(H), to proton translocation:

$$NADH + NADP^+ + H^+_{out} \leftrightarrow NAD^+ + NADPH + H^+_{in} \quad (1)$$

where H^+_{out} and H^+_{in} denote hydrogen ions outside and inside the intact coupling membrane system (Fig. 1, and for review see [15,16]). Transhydrogenase has three structural components: dI, which binds NAD^+ and NADH, and dIII, which binds $NADP^+$ and NADPH, both protrude from the membrane (towards the matrix in mitochondria,

* Corresponding author.
E-mail address: J.B.JACKSON@bham.ac.uk (J.B. Jackson).
[1] These authors contributed equally to this work.

0005-2728/$ – see front matter © 2010 Elsevier B.V. All rights reserved.
doi:10.1016/j.bbabio.2010.01.006

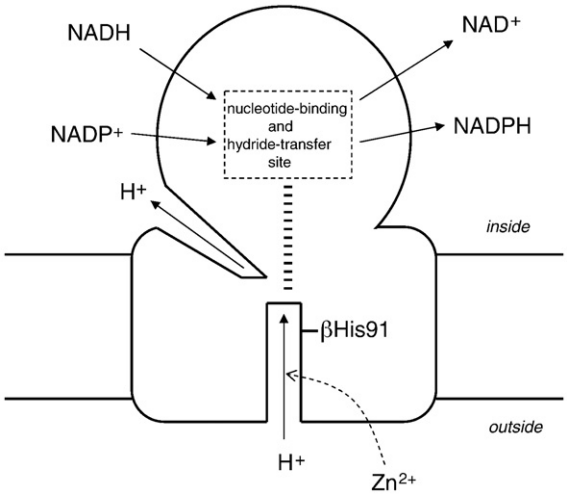

Fig. 1. Inhibition by Zn^{2+} of proton transfer through transhydrogenase. *Inside* and *outside* refer to the aqueous phases on either side of the intact membrane. The reaction is shown as proceeding in the "forward" direction. The ladder of short horizontal lines represents the transmission of a conformational change from the proton-transfer pathway to the nucleotide-binding and hydride-transfer site. βHis91 is located in the putative transmembrane helix 9 in dII [25].

and the cytoplasm in bacteria), while dII spans the membrane. High-resolution crystallographic structures are available for dI [17,18], dIII [19,20] and dI–dIII complexes [21], but not for dII.

In membrane vesicles from *Escherichia coli* and *Rhodospirillum rubrum*, Zn^{2+} inhibits forward and reverse transhydrogenation (see Eq. (1)) but, depending on pH, has either no effect on, or stimulates "cyclic" transhydrogenation, a partial reaction in which $NADP^+$ and NADPH remain bound to the enzyme, and which is not coupled to proton translocation across the membrane [13]. These differential effects led to the conclusion that the metal ion interferes specifically with proton-translocation steps associated with binding and release of $NADP^+$/NADPH. It was suggested that Zn^{2+} binds to a site in the proton-transfer pathway, and blocks translocation, as in the photosynthetic reaction center. Consistent with this view, attenuated total-reflectance Fourier-transform infrared (ATR-FTIR) difference spectroscopy indicated that His and Asp/Glu residues are involved in the Zn^{2+}-binding cluster [14].

βHis91, a residue well-conserved across species and located in the membrane-spanning domain of transhydrogenase (see Fig. 1), was proposed to play an important role in the enzyme's turnover, possibly participating in proton translocation [14,22–26]. A mutant in which βHis91 was replaced by Lys exhibited greatly reduced forward and reverse transhydrogenation and stimulated the cyclic reaction, thus mimicking the effects of Zn^{2+} treatment of the wild-type enzyme [14,23,25,26]. Zn^{2+}-induced ATR-FTIR difference spectra of the βH91K mutant also revealed contributions from His and carboxylate residues, but the signal amplitudes were significantly lower than those in wild-type enzyme, particularly in the spectral region attributable to His [14]. These observations led to the suggestion that Zn^{2+} binding and the βHis91→Lys substitution inhibit proton translocation at the same or neighbouring sites, and that the imidazole side chain of βH91 might provide a ligand for the metal ion.

X-ray absorption fine structure (XAFS) is a useful tool for probing the local structure of a metal ion in a protein since it can be applied to non crystalline samples and can provide structural information at subatomic resolution (<0.2 Å) (eg [27]). In this communication we present an XAFS analysis of Zn^{2+}-binding sites in purified transhydrogenase complexes from *E. coli*. In order to test the possible involvement of βHis91 in coordinating the metal, we have analyzed XAFS spectra acquired with the wild-type enzyme and with the βH91K mutant. A single Zn^{2+}-binding cluster formed by one Cys, two His and one Asp/Glu residue, arranged in the same tetrahedral coordination geometry, best accounts for the XAFS spectra of both the wild-type and the mutant transhydrogenase, indicating that βHis91 does not directly participate in the binding site.

2. Materials and methods

2.1. Sample preparation

Wild-type *E. coli* transhydrogenase and its βH91K mutant, each carrying a cleavable His tag at the N-terminus of the α subunit, were expressed from pSI4 and pSI5, respectively, and purified by Ni^{2+} chromatography, as described [14]. Precautions were taken to limit contamination of the protein by metal ions in the buffer solutions, as indicated in the earlier report. The tag was removed from both proteins with Factor Xa, and the transhydrogenases were separated from the cleavage enzyme and products by gel permeation chromatography [14]. Protein quantities were determined using the bicinchoninic acid assay [28], and are given below in mol of "dI–dII–dIII monomer". The proteins were stored in 50 mM HEPES-KOH, pH 7.5, 0.2 M NaCl, 0.05% $Anapoe_{35}$, 25% w/v glycerol at −20 °C, as described [14]. Following storage the proteins (0.10 µmol wild-type protein in 20 mL of storage buffer, and 0.11 µmol βH91K in 15 mL) were dialysed against 50 mM HEPES-KOH, pH 8.2, 2 mM $MgCl_2$ 0.05% $Anapoe_{35}$. The two proteins were concentrated to a volume of approx 1.5 mL using Vivascience 100 k cut-off filters, and then further dialysed against similar buffer before concentrating to approx 0.6 mL.

The wild-type and mutant transhydrogenases were each mixed with appropriate stock solutions to give 1.0 mL of 45 µM protein, 3.3% w/v polyvinyl alcohol (PVA, Mr≈130,000, Fluka), 50 mM HEPES-KOH, pH 8.2, 2 mM $MgCl_2$, 0.05% $Anapoe_{35}$. Separate 1.0 mL samples, identical to these but for the presence of 36 µM added $ZnCl_2$, were also prepared. The four solutions were each transferred to $3\times3\times0.3$ cm^3 Teflon holders, and dehydrated under dry nitrogen flow, incurring a volume decrease of about 10 fold. The incorporation of membrane complexes at high concentration into PVA films yields samples that are stable and easy to handle [6,10].

Thermolysin (TLS) and superoxide dismutase (SOD) from bovine erythrocytes were purchased from Calbiochem and Sigma-Aldrich, respectively. TLS was re-crystallized as described in [29]. Films were prepared by adding 350 µl of a 10% w/v solution of PVA to 1 mL of 20 mM Ca-acetate, pH 7.5 containing 15 mg TLS and to 1 mL of 50 mM Tris–HCl, pH 7.5 containing 3 mg SOD. The solutions were dehydrated under nitrogen as described above.

2.2. Transhydrogenation assay

Rates of reverse transhydrogenation by the purified, detagged protein were measured by recording the reduction of acetyl pyridine adenine dinucleotide ($AcPdAD^+$, 200 µM) by NADPH (200 µM) in 50 mM HEPES, pH 7.2, 2 mM $MgCl_2$, 0.01% $Anapoe_{35}$ (see [14]). Rates of cyclic transhydrogenation were measured from the reduction of $AcPdAD^+$ (200 µM) by NADH (200 µM) in the presence of $NADP^+$ (50 µM) in the same buffer. The reaction rates were similar to those measured under similar conditions in previous work [14].

2.3. XAFS data collection and analysis

Experimental Zn K-edge spectra of the protein films were collected at beamline GILDA-BM08 [30] of the European Synchrotron Radiation Facility. A Si(311) double crystal monochromator employing dynamical sagittal focussing [31] was used. The spot size was approximately 1×1 mm^2 and the flux on the sample 3×10^{10} photons s^{-1}. Data were collected at 80 K, using a 13-element hyper-pure Ge detector equipped with fast digital electronics and a peaking time of 1 µs [32]. The total

integration time was 45 s/point for the two samples with added Zn and 90 s/point for samples without added Zn.

In order to check for possible modifications in the local structure of the Zn site caused by irradiation during the measurement, we compared 5 consecutive spectra that had been acquired on the same position of samples containing the wild-type transhydrogenase and its βH91K mutant. In each case, the first XANES spectrum, which required an acquisition time of 20 min, was indistinguishable from the spectra acquired subsequently; this suggests that radiation damage was not significant. Similarly, no changes were detected in consecutive spectra in the EXAFS region, even after an exposure of 8 h.

EXAFS spectra were extracted from the raw data using the Autobk algorithm [33] implemented in the Athena package [34], and then fitted with Artemis 0.8.013 [34]. Theoretical scattering amplitudes and phase shifts were calculated by means of the *ab initio* code FEFF8.2 [35], including Self Consistent Field calculations for the potential in a radius of 4.8 Å around the absorber. All of the multiple scattering signals arising from up to five single scattering events relative to the same amino acid and with an effective length ≤5 Å were taken into account in the fitting procedure. The amplitude reduction factor S_0^2 was calculated from atomic overlap integrals by the program: its value was fixed to 0.95 during the analysis.

Input clusters for FEFF8.2 were built using MOLDRAW [36] for visualization and manipulation, setting first neighbour distances to the target values provided by M. M. Harding (see [37] and references therein) and interatomic distances and angles relative to each amino acid to the values provided by Engh and Huber [38]. Initial Debye Waller (DW) factors values were derived from the parameterization provided by Dimakis and Bunker as a result of Density Functional Theory calculations [39]. Fits were performed directly in *k* space, with a *k* weight of 3, in the range 2.5–12.5 $Å^{-1}$, minimizing the *R* factor, defined as:

$$R = \sum_{i=1,N} (k_i^3 \tilde{\chi}_{i_{data}} - k_i^3 \tilde{\chi}_{i_{fit}})^2 \Big/ \sum_{i=1,N} (k_i^3 \tilde{\chi}_{i_{data}})^2$$

where $\tilde{X}_i$ are the values of the EXAFS function, and *N* is the total number of experimental points. The Rigid Body Refinement scheme was applied [40].

Simulations of XANES spectra were performed using the Finite Difference Method implemented in the FDMNES program [41].

3. Results

PVA films of intact, purified, detergent-dispersed transhydrogenase from *E. coli* were prepared in the absence and presence of $ZnCl_2$. From titrations of the inhibitory effect of Zn^{2+} on the rate of reverse transhydrogenation the K_d for the metal ion is 2.5 μM at pH 8.2 [14]. Assuming for the moment that there is only one metal-ion binding site per protein monomer then, in the solutions used to prepare the films (45 μM protein, 36 μM $ZnCl_2$), 68% of the Zn^{2+} sites would be occupied and the concentration of free Zn^{2+} (or Zn^{2+} bound to water molecules) would be 5.4 μM. During dehydration of the film the volume reduction will have led to an increase in binding, and a corresponding decrease in the amount of free Zn^{2+}. This should ensure that the contribution of free metal ion to the XAFS spectra is negligible (and see below).

XAFS spectra were acquired in films containing wild-type transhydrogenase and its βH91K mutant in the absence (samples designated WT and BH91K, respectively) and presence of added Zn ions (WT-Zn and BH91K-Zn, respectively) — Figs. 2 and 3. There was much lower but nevertheless significant Zn K_α fluorescence in the two samples prepared without added Zn^{2+} indicating a low level of contaminating metal ion in both the wild-type and βH91K proteins. Because the film thickness was not homogeneous, and because fluorescence is strongly affected by experimental geometry, these data cannot be used to evaluate accurately the amount of contaminating Zn^{2+}. We therefore used a functional assay of the purified protein in solution to show that the amount of the bound metal ion is indeed very low. Firstly, we confirmed that the inhibitory effect of added Zn^{2+} (50 μM) on reverse transhydrogenase, and the stimulatory effect of the metal ion on cyclic transhydrogenation, were relieved (by 85%) upon subsequent addition of 200 μM EDTA [13,14]. This shows that the EDTA effectively removes Zn^{2+} from the inhibitory site on the enzyme. Then in duplicate samples of purified transhydrogenase in the absence of added Zn^{2+}, we found that 200 μM EDTA neither stimulated the rate of reverse transhydrogenation nor inhibited the rate of the cyclic reaction. This shows that the amount of contaminating Zn^{2+} bound to the transhydrogenase under assay conditions is less than the error in the rate measurements (approx 5%, see [14]).

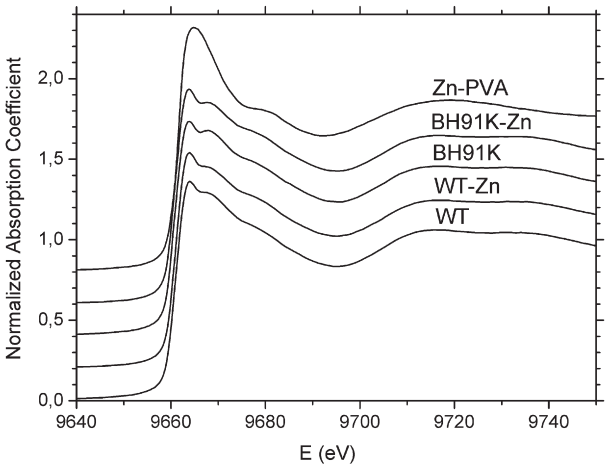

Fig. 2. Experimental XANES spectra. K-edge Zn XANES spectra for wild-type transhydrogenase without and with added Zn^{2+} (WT and WT-Zn, respectively), for its βH91K mutant without and with added Zn^{2+} (BH91K and BH91K-Zn, respectively), and for a reference sample obtained by embedding $ZnCl_2$ in a PVA matrix (Zn-PVA). All spectra were measured at 80 K.

The near-edge regions of the spectra (XANES, Fig. 2) and the EXAFS functions (Fig. 3) were very similar for all four samples indicating just a single class of Zn^{2+}-binding sites. Evidently the sites are similar in the

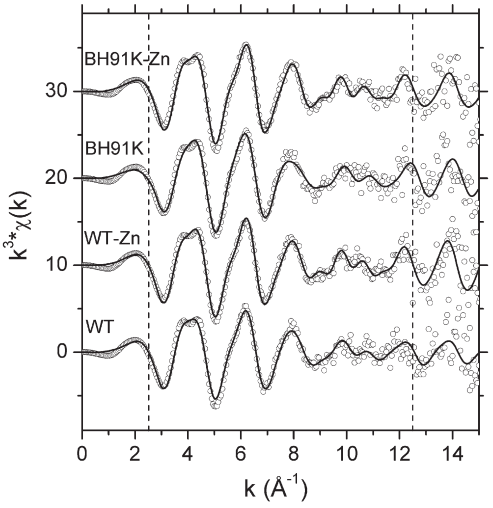

Fig. 3. The experimental EXAFS spectra and their fits based on the 1Cys 2His 1Asp/Glu model. Zn K-edge EXAFS spectra for wild-type transhydrogenase without and with added Zn^{2+} (WT and WT-Zn, respectively), and for its βH91K mutant without and with added Zn^{2+} (BH91K and BH91K-Zn, respectively), measured at 80 K (circles). For each spectrum the continuous line shows the corresponding *k*-space best fit. Dashed lines indicate the fitting range 2.5–12.5 $Å^{-1}$.

wild-type protein and the βH91K mutant and, moreover, the contaminating Zn^{2+} populates a small fraction of the sites occupied by the added metal ion. In Fig. 2 we also show the XANES spectrum of a sample made of $ZnCl_2$ embedded in PVA in the absence of protein (Zn-PVA). The higher white-line intensity and the lack of inflection points after the white line and up to 9675 eV make this markedly different from the XANES spectra of the transhydrogenase samples. This difference indicates that there is no significant contribution from PVA-bound Zn in the spectra of the transhydrogenase samples. It suggests that essentially all the metal ions detected by XAS in the transhydrogenase samples are bound to the protein and that contributions from unbound ions dispersed in the PVA matrix are negligible.

Information on the coordination number of Zn^{2+} in the transhydrogenase samples can be obtained by comparing the observed XANES spectra with those simulated using the commonest high-resolution structures in the Protein Data Bank with 4-, 5-, and 6-coordinated Zn sites [42]. Consistent with experimental data [43], simulations of XANES spectra show that the white-line intensity increased with the coordination number. In particular we observed that the maximum of the simulated absorption coefficient was never higher than 1.5 when Zn occupies a tetrahedral site, in agreement with [43]. A white-line intensity lower than 1.6 was never observed for coordination numbers of 5 and 6. In all the transhydrogenase samples examined the maximum absorption coefficient was lower than 1.5, indicating that the Zn^{2+} is 4-coordinated.

The relative number of S atoms and N/O atoms in the Zn coordination sphere can be determined by an *R*-space first-shell fit. In our calculations the number of S atoms, *n*, was a free parameter of the fit, while the total number of Zn neighbours was set to 4. The remaining $(4-n)$ atoms could be either N or O; we did not try to distinguish between these low atomic number ligands at this stage of the analysis, since their contributions to the first-shell signal are very similar and easily mistaken [44]. Zn–S and Zn–N/O distances were also free variables of the fit and their convergence to reasonable values was checked. The fourth and last free parameter in these fits was a common shift in the energy origin (ΔE_0) of the included scattering paths. In our analysis DW factors were fixed to values calculated from the parameterization provided in [39]. The Fourier transformed (FT) EXAFS spectrum for WT-Zn is shown in Fig. 4 (empty circles), together with its first-shell fit performed in the *R* region, 1.0–2.2 Å (continuous line). According to the fit results, indicating the presence of 0.9 ± 0.1 S atoms, and consequently 3.1 ± 0.1 N/O, we expect Zn^{2+} to bind 1 Cys and 3 more ligands to be identified most probably from His, carboxylic acids and water molecules [45]. We propose that the S atom can indeed be assigned to a Cys residue on the basis of a Metalloprotein Database and Browser (MDB) search (http://metallo.scripps.edu/): where S atoms provide a ligand for Zn^{2+}, they are always located in Cys residues, never Met.

The imidazole ring of His is the only structure amongst possible Zn^{2+} ligands which can contribute significantly to the Multiple Scattering paths responsible for the signal at high *R* values [46]. Therefore, an inspection of the 3–4 Å region of the FT spectrum can provide information on the number of His residues present in the cluster. We compared the transhydrogenase FT spectrum with those of reference samples recorded in similar experimental conditions, and in which the number of His residues per Zn^{2+} cluster is known. The chosen reference proteins were Thermolysin (TLS) and Superoxide Dismutase (SOD). As shown by X-ray crystallography, and confirmed by XAFS analysis, TLS binds a Zn ion, coordinated by 2 His, 1Glu and 1 water molecule [47], while the Zn ion bound to SOD is coordinated by 3 His and 1 Asp [48]. The FT spectra reported in Fig. 4 clearly show that the amplitude of the MS contribution in the 3–4 Å region of the WT-Zn transhydrogenase spectrum is comparable to that of TLS. Measuring the amplitude of these contributions by numerical integration in the region 3–4 Å we obtain a value of 1.20 for the WT-Zn spectrum, very close to the value of 1.29 calculated for TLS and markedly different

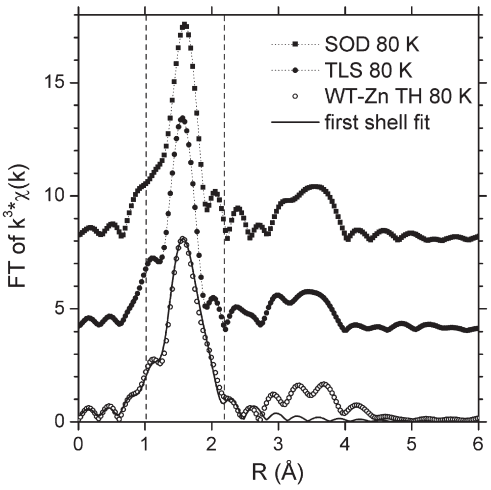

Fig. 4. Experimental Fourier Transformed EXAFS spectra of model proteins and wild-type transhydrogenase, and its first-shell fit. The Fourier Transformed K-edge Zn spectra of wild-type transhydrogenase with added Zn^{2+} (open circles), superoxide dismutase (filled squares), and of thermolysin (filled circles), embedded in PVA films, are shown. The spectra were collected at 80 K and transformed in the *k* range 2.5–12.5 $Å^{-1}$. The continuous line shows the first-shell fit for the transhydrogenase spectrum; the fitting range 1–2.2 Å is indicated by the dashed lines.

from the value of 1.85 obtained for SOD. We can therefore assume that Zn^{2+} in the WT-Zn sample is bonded to 2 His residues, like the Zn^{2+} of TLS. The fourth ligand could be either a carboxylic acid residue or a water molecule, but since ATR-FTIR experiments indicated a change in the vibrational modes of Asp/Glu residues upon Zn^{2+} binding [14], it is reasonable to assume the presence of an Asp/Glu in the Zn^{2+} coordination shell.

We therefore chose a 1Cys 2His 1Asp/Glu coordination shell as a starting model. In order to minimize the correlation between the fitting parameters, the fit to the EXAFS function in *k* space was performed in a step-by-step procedure [49]. In step (1) the free parameters of the fit were three first-shell distances (one for each different amino acid residue), and the bending angle of Asp/Glu, while the DW factors were fixed. In step (2) first-shell distances were fixed to the best-fit values of the previous fitting step and the DW factors were allowed to vary: the free parameters of the fit were then first-shell Single Scattering (SS) DWs and a common value, σ^2_{MS}, for all of the Multiple Scattering (MS) paths. In step (3) DWs were set to the best-fit values of step (2) and first-shell distances were allowed to vary. When fitting the EXAFS spectra measured in the experimental samples the distances obtained in step (3) always converged to values that were in close agreement with those found in step (1), proving the robustness of the fitting procedure. In all fitting steps a shift in the energy origin (ΔE_0) was included as a free parameter.

The fitting model was chosen and tested on the WT-Zn data, and then extended to that from the other experiments. The fits for all four samples are shown in Fig. 3 as continuous lines. The agreement between the fitting curve and the experimental signal is good, particularly in the WT-Zn and BH91K-Zn samples, where the signal-to-noise ratio (S/N) is higher as a consequence of the higher Zn fluorescence counts. The slight inaccuracy in reproducing the high-frequency oscillation at 4 $Å^{-1}$ is related to multiple scattering contributions. It probably arises because intra-ligand paths were not included in the model. The best-fit first-shell distances (i.e. the output of step 3 of the fitting procedure) relative to the model, 1Cys 2His 1Asp/Glu, are reported in Table 1. The corresponding DW factors (i.e. the output of step 2) are given in Table 2. First-shell distances are the same within the error in all samples except in BH91K, which has a slightly shorter first-shell average distance. The fact that the same

Table 1
Best-fit first-shell distances. First-shell distances were obtained by fitting the EXAFS spectra of the four samples to the 1Cys 2His 1Asp/Glu model described in the text. The parameter α is the angle Zn-$O_{\delta1}$-C_γ or Zn-$O_{\varepsilon1}$-C_δ of the Asp/Glu residue, respectively, and whose starting value is set to 105°. A common distance for Zn-$N_{\varepsilon2}$ has been assigned to the two His residues, and this therefore indicates the average of the two actual distances. The values in brackets are the 1σ errors.

	ΔE_0 (eV)	Zn–S (Å)	Zn–$N_{\varepsilon2}$ (Å)	Zn–$O_{\delta1/\varepsilon1}$ (Å)	α (°)	R_{factor} (%)
WT	−2.7 (1.3)	2.288 (0.013)	2.016 (0.016)	1.972 (0.025)	112 (3)	7.2
WT-Zn	−2.4 (1.0)	2.290 (0.009)	2.018 (0.014)	1.969 (0.015)	114 (2)	6.1
BH91K	−4.6 (1.5)	2.268 (0.011)	1.976 (0.013)	1.99 (0.03)	106 (1)	7.3
BH91K-Zn	−2.0 (0.8)	2.287 (0.007)	2.018 (0.010)	1.968 (0.015)	113 (2)	4.8

model provides a good fit for WT and WT-Zn, as well as for BH91K and BH91K-Zn, confirms that the contaminating Zn^{2+} in the samples with no exogenous metal ion populates a fraction of the same site resolved in the presence of added Zn^{2+}.

Since the same cluster of residues nicely fits the signals measured in samples containing the native and the mutant transhydrogenase, we are led to think that the Zn^{2+}-binding site is indeed the same, i.e. that the mutated βHis91 is not involved in the binding cluster. If it were, the spectrum of the BH91K-Zn sample would differ from that of WT-Zn, and it would reveal a Lys residue instead of one of the His ligands in the coordinating cluster. In order to test quantitatively this possibility we have fitted the BH91K-Zn spectrum with the model, 1Cys 1His 1Lys 1Asp/Glu. Fig. 5 compares the best fit to the two models. It clearly shows that the Lys-containing cluster gives a poorer fit to the spectrum. This is particularly evident when comparing the FT signals (lower panel): the 1Cys 1His 1Lys 1Asp/Glu model (indicated with LYS in the figure) gives a worse fit to the experimental data than the 1Cys 2His 1Asp/Glu model (indicated with HIS), both in the first shell and in the 3–4 Å region where the His contributions are predominant. In fact, the *R* factor of the fit increases from 4.8% to 7.1% when a His is replaced with a Lys. The inadequacy of the LYS model is further illustrated by the best-fit value found for the DW factor common to all MS paths, i.e. $\sigma^2_{MS} = 0.000 \pm 0.002$ Å^2. The DW factors and the amplitude reduction factor S_0^2 are correlated fit parameters; the value of $S_0^2 = 0.95$ was calculated and then fixed during the analysis — this could affect the resulting values of the DWs. Although a value of 0.95 is quite reasonable for S_0^2, we have tested the effect of varying this value on the DW factors. Thus, we fitted the BH91K-Zn spectrum to the 1Cys 1His 1Lys 1Asp/Glu model setting S_0^2 to 0.8, a lower but still reasonable value. This procedure led again to the best-fit value $\sigma^2_{MS} = 0.000 \pm 0.002$ Å^2, but to a worse fit, as indicated by the *R* factor of 8.6%. The result of a null multiple scattering DW factor, independent of the choice of the S_0^2 value, would lack physical meaning. It would indicate that the MS contributions relative to the LYS model are too weak to reproduce the experimental spectrum, and that they could fit only if they were not damped (i.e. associated to a null Debye Waller factor).

The differences in the *R* factors and in the reduced chi squared values (53 ± 16 and 130 ± 40, respectively, for the HIS and LYS models) are at the limit of resolution from a statistical point of view (see [10] and references therein). However, all the evidence reported above strongly supports the idea that the Zn^{2+}-binding site does not involve a Lys residue. Moreover, if one of the two His residues present in the Zn^{2+}-binding motif of wild-type transhydrogenase were replaced by another ligand in the mutant, we would encounter differences in the XANES regions of the spectra. However, these regions are nearly identical to one another (Fig. 2). Finally, we must in principle consider also the possibility that in the βH91K mutant Zn^{2+} loses one of its ligands and results in a coordination number of 3. In fact, if βHis91 were one of the Zn^{2+} ligands in the wild-type protein, its substitution with a Lys would introduce a positively charged amino acid into the coordination sphere, which would clearly have a lower propensity to bind Zn^{2+}. This possibility can however be excluded because a decrease in the coordination number would cause a significant decrease in the EXAFS oscillation amplitude and in the XANES white-line intensity which we do not observe at all in the BH91K spectra. In conclusion, XANES and EXAFS analysis identifies the same Zn^{2+}-binding cluster, formed by 1Cys, 2His, and 1Asp/Glu residue in the native transhydrogenase and in its βH91K mutant (see Fig. 6). This strongly argues against an involvement of βHis91 in the Zn^{2+}-binding site that is detected by XAFS.

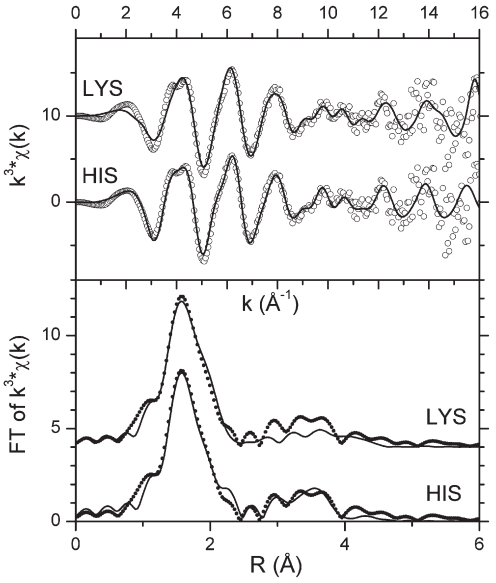

Fig. 5. The EXAFS spectrum of Zn in the βH91K mutant of transhydrogenase fitted with two different models. Upper panel: the experimental Zn K-edge EXAFS spectrum of the BH91K-Zn sample (open circles) and its *k*-space fits (continuous lines) based on the 1Cys 1His 1Lys 1Asp/Glu model (indicated by the tag LYS), and the 1Cys 2His 1Asp/Glu model (indicated by HIS). Lower panel: Fourier Transforms of the experimental spectra (black dots) and of the fits (continuous lines) shown in the upper panel.

Table 2
Best-fit Debye Waller factors. First-shell Single Scattering Debye Waller factors and a Multiple Scattering DW common to all MS paths, as determined by fitting the four EXAFS spectra with the 1Cys 2His 1Asp/Glu model. The subscripts relative to $N\varepsilon_2$ of His and $O_{\delta1}/O_{\varepsilon1}$ of Asp/Glu have been omitted. The values in brackets are the 1σ errors.

	σ^2_{Zn-S} (10^{-3} Å^2)	σ^2_{Zn-N} (10^{-3} Å^2)	σ^2_{Zn-O} (10^{-3} Å^2)	σ^2_{MS} (10^{-3} Å^2)	R_{factor} (%)
WT	3.9 (1.0)	3.5 (2.5)	5 (5)	7.6 (2.2)	7.2
WT-Zn	3.1 (0.7)	4 (3)	2 (4)	4.4 (1.1)	6.2
BH91K	2.3 (0.8)	3.1 (1.4)	4.0 (2.0)	6.9 (2.5)	7.2
BH91K-Zn	2.3 (0.6)	2.9 (1.4)	3.6 (2.3)	4.5 (1.0)	4.8

4. Discussion

The Zn K-edge XAS spectra of purified *E. coli* transhydrogenase described above were interpreted in terms of a single Zn^{2+}-binding site. The existence of two (or more) sites with different structures and binding affinities is unlikely: it would contradict the finding that spectra obtained with low levels of contaminating Zn^{2+} have very similar features to those obtained with much higher concentrations of the metal ion. Thus, even small differences in binding affinity would lead to significant changes in the relative site occupation, to which XAS is rather sensitive. The existence of two structurally different sites with identical Zn^{2+}-binding affinities is not ruled out by these observations but would be difficult to reconcile with the internal consistencies of the XAS analysis, notably the convergence of results from different fitting procedures. It is likely therefore that there is indeed only a single site in

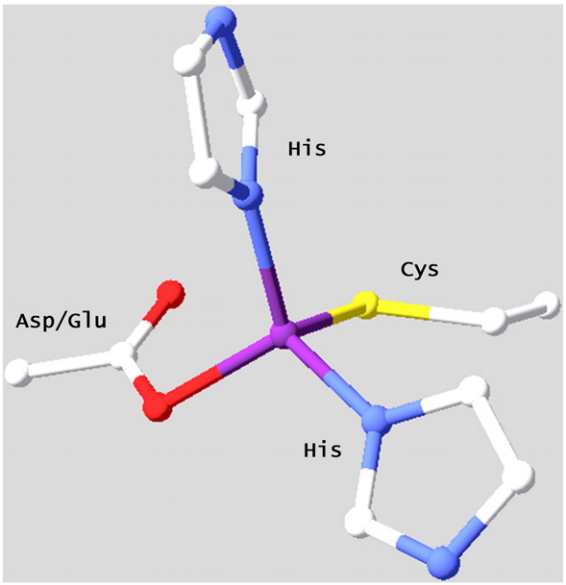

Fig. 6. The proposed Zn^{2+}-binding cluster. Wireframe structure of the Zn^{2+}-binding cluster which gives the best fit of the experimental XAFS data obtained for both the wild-type transhydrogenase and its βH91K mutant.

transhydrogenase that binds Zn^{2+} in the concentration range of our experiments; the XAS experiments indicate that the site is a tetrahedral cluster formed by the imidazole rings of two His residues, and the side chains of a Cys and an Asp/Glu. We propose that Zn^{2+} inhibition of proton translocation by transhydrogenase [13,14] is a consequence of the metal ion binding to this site. In the absence of metal ions, one or more of the amino acid residues in the cluster may be involved in proton transfer, and Zn^{2+} would inhibit by competing with H^+ binding to the site. The inhibitory Zn^{2+}-binding sites in reaction centers of *Rhodobacter sphaeroides* [5,6], and in avian and bovine cytochrome bc_1 complexes [10] also have two His and one Asp/Glu residues, and these sites too are thought to be involved in proton transfer and to bind the metal ion competitively.

Mutation of βHis91 to Lys was found to have somewhat similar effects on transhydrogenase reactions to treatment of the enzyme with Zn^{2+} [14]. An analysis of these effects led to the conclusion that both the amino acid substitution, and metal-ion binding, interfere with proton translocation. In other experiments the addition of Zn^{2+} to wild-type transhydrogenase led to changes in the ATR-FTIR difference spectrum that were attributable to effects on His and Asp/Glu residues in the protein [14]. In the βH91K mutant the amplitude of the signals due to Asp/Glu, and particularly those due to His, in the Zn^{2+}-induced difference spectrum was decreased prompting the suggestion that βHis91 in wild-type transhydrogenase might be a ligand for the Zn^{2+}. However, in the present study we found that the Zn XANES and EXAFS spectra were very similar in the wild-type and in the βH91K mutant. The same binding cluster of 1Cys, 2His and 1Asp/Glu residue provides the best fit for both sets of data. An alternative model, a 1Cys, 1His, 1Lys, and 1Asp/Glu Zn^{2+}-binding cluster, yielded a worse fit to the measured spectra of the mutant protein. The inadequacy of the "mutated" cluster was particularly evident in the spectral region dominated by the His contributions. It is very unlikely that βHis91 participates directly in Zn^{2+}-binding.

The Zn^{2+}-binding site in dII is on the inside of the intact membrane (the *n*-side) [14] — see Fig. 1. Although there is currently no high-resolution structure of the membrane-spanning dII component of transhydrogenase, hydropathy profiles and biochemical experiments have led to a topology model of the *E. coli* enzyme [50]. If we assume that amino acid residues in the site are located close to the interface between the inside aqueous phase and the membrane dielectric, and we allow for some uncertainty in the position of the transmembrane helices in the model, then the side chains of Cys397, Cys435, His447, and His450 in the α subunit, and His27, Glu28, Glu79, Glu82, Glu85, Cys147, His204, Asp213 and Cys260 in the β subunit are candidates for the Zn^{2+}-binding ligands.

It seems that, although βHis91 and the Zn^{2+}-sensitive site both function in the proton-translocation pathway of transhydrogenase, they are spatially separate. Indeed, it was noted [14] that the low residual rate of reverse transhydrogenation in βH91K was further inhibited by Zn^{2+}, and that the elevated rate of cyclic transhydrogenation in the mutant was further stimulated by metal ions. To reconcile the present XAFS results with the effects of the βHis91 → Lys mutation on the Zn^{2+}-induced FTIR difference spectra [14] we propose the following. The binding of Zn^{2+} to a site in transhydrogenase dII formed by 1Cys 2His and 1Asp/Glu, causes structural changes that are transmitted to the somewhat more distant βHis91 residue. The FTIR difference spectra detect these changes in βHis91 as well as those arising from one or both of the His residues which form the binding site. When βHis91 is mutated into a Lys, Zn^{2+} binding still perturbs the vibrational bands of the His residue(s) that act as ligand (s), but the absence of the contribution from βHis91 causes the observed decrease in the overall His FTIR signal.

Acknowledgements

This work was supported by MIUR of Italy and by the Biotechnology and Biological Sciences Research Council in the UK. Measurements at ESRF were performed within the public user program. We are grateful to the staff of the GILDA beamline of ESRF for excellent support.

References

[1] T.A. Link, G. von Jagow, Zinc ions inhibit the Q_P center of bovine heart mitochondrial bc_1 complex by blocking a protonatable group, J. Biol. Chem. 270 (1995) 25001–25006.
[2] K. Faxén, L. Salomonsson, P. Adelroth, P. Brzezinski, Inhibition of proton pumping by zinc ions during specific reaction steps in cytochrome *c* oxidase, Biochim. Biophys. Acta 1757 (2006) 388–394.
[3] D.A. Mills, B. Schmidt, C. Hiser, E. Westley, S. Ferguson-Miller, Membrane-potential-controlled inhibition of cytochrome oxidase by zinc, J. Biol. Chem. 277 (2002) 14894–14901.
[4] M.L. Paddock, M.S. Graige, G. Feher, M.Y. Okamura, Identification of the proton pathway in bacterial reaction centers: inhibition of proton transfer by binding of Zn^{2+} or Cd^{2+}, Proc. Natl. Acad. Sci. U. S. A. 96 (1999) 6183–6188.
[5] H.L. Axelrod, E.C. Abresch, M.L. Paddock, M.Y. Okamura, G. Feher, Determination of the binding sites of the proton transfer inhibitors Cd^{2+} and Zn^{2+} in bacterial reaction centers, Proc. Natl. Acad. Sci. U. S. A. 97 (2000) 1542–1547.
[6] L. Giachini, F. Francia, A. Mallardi, G. Palazzo, E. Carpené, F. Boscherini, G. Venturoli, Multiple scattering X-ray absorption studies of Zn^{2+} binding sites in bacterial photosynthetic reaction centers, Biophys. J. 88 (2005) 2038–2046.
[7] M.L. Paddock, L. Sagle, A. Tehrani, J.T. Beatty, G. Feher, M.Y. Okamura, Mechanism of proton transfer inhibition by Cd^{2+} binding to bacterial reaction centers: determination of the pK_A of functionally important histidine residues, Biochemistry 42 (2003) 9626–9632.
[8] S.S. Klishin, W. Junge, A.Y. Mulkidjanian, Flash-induced turnover of the cytochrome bc_1 complex in chromatophores of *Rhodobacter capsulatus*: binding of Zn^{2+} decelerates likewise the oxidation of cytochrome *b*, the reduction of cytochrome c_1 and the voltage generation,, Biochim. Biophys. Acta 1553 (2002) 177–182.
[9] E.A. Berry, Z. Zhang, H.D. Bellamy, L. Huang, Crystallographic location of two Zn^{2+}-binding sites in the avian cytochrome bc_1 complex, Biochim. Biophys. Acta 1459 (2000) 440–448.
[10] L. Giachini, F. Francia, G. Veronesi, D.-W. Lee, F. Daldal, L.-S. Huang, E.A. Berry, T. Cocco, S. Papa, F. Boscherini, G. Venturoli, X-ray absorption studies of Zn^{2+} binding sites in bacterial, avian, and bovine cytochrome bc_1 complexes, Biophys. J. 93 (2007) 2934–2951.
[11] K. Muramoto, K. Hirata, K. Shinzawa-Itoh, S. Yoko-o, E. Yamashita, H. Aoyama, T. Tsukihara, S. Yoshikawa, A histidine residue acting as a controlling site for dioxygen reduction and proton pumping by cytochrome *c* oxidase, Proc. Natl. Acad. Sci. U. S. A. 104 (2007) 7881–7886.
[12] F. Francia, L. Giachini, F. Boscherini, G. Venturoli, G. Capitanio, P.L. Martino, S. Papa, The inhibitory binding site(s) of Zn^{2+} in cytochrome *c* oxidase, FEBS Lett. 581 (2007) 611–616.
[13] S.J. Whitehead, K.E. Rossington, A. Hafiz, N.P. Cotton, J.B. Jackson, Zinc ions selectively inhibit steps associated with binding and release of NADP(H) during

turnover of proton-translocating transhydrogenase, FEBS Lett. 579 (2005) 2863–2867.
[14] S.J. Whitehead, M. Iwaki, N.P.J. Cotton, P.R. Rich, J.B. Jackson, Inhibition of proton-transfer steps in transhydrogenase by transition metal ions, Biochim. Biophys. Acta 1787 (2009) 1276–1288.
[15] J.B. Jackson, Proton translocation by transhydrogenase, FEBS Lett. 545 (2003) 18–24.
[16] J.B. Jackson, S.A. White, T.H.C. Brondijk, Hydride transfer and proton translocation by nicotinamide nucleotide transhydrogenase, in: M. Wikstrom (Ed.), Biophysical and Structural Aspects of Bioenergetics, Royal Society of Chemistry, Cambridge, 2005, pp. 376–393.
[17] P.A. Buckley, J.B. Jackson, T. Schneider, S.A. White, D.W. Rice, P.J. Baker, Protein–protein recognition, hydride transfer and proton pumping in the transhydrogenase complex, Structure 8 (2000) 809–815.
[18] T. Johansson, C. Oswald, A. Pedersen, S. Tornroth, M. Okvist, B.G. Karlsson, J. Rydstrom, X-ray structure of domain I of the proton-pumping membrane protein transhydrogenase from *Escherichia coli*, J. Mol. Biol. 352 (2005) 299–312.
[19] G.S. Prasad, V. Sridhar, M. Yamaguchi, Y. Hatefi, C.D. Stout, Crystal structure of transhydrogenase domain III at 1.2 A resolution, Nat. Struct. Biol. 6 (1999) 1126–1131.
[20] S.A. White, S.J. Peake, S. McSweeney, G. Leonard, N.P.J. Cotton, J.B. Jackson, The high resolution structure of the NADP(H)-binding component of proton-translocating transhydrogenase from human-heart mitochondria, Structure 8 (2000) 1–12.
[21] T. Bhakta, S.J. Whitehead, J.S. Snaith, T.R. Dafforn, J. Wilkie, S. Rajesh, S.A. White, J.B. Jackson, Structures of the dI_2dIII_1 complex of proton-translocating transhydrogenase with bound, inactive analogues of NADH and NADPH reveal active-site geometries, J. Biol. Chem. 46 (2007) 3304–3318.
[22] N.A. Glavas, C. Hou, P.D. Bragg, Involvement of histidine-91 of the beta subunit in proton translocation by the pyridine nucleotide transhydrogenase of *Escherichia coli*, Biochemistry 34 (1995) 7694–7702.
[23] N.A. Glavas, P.D. Bragg, The mechanism of hydride transfer between NADH and 3-acetyl pyridine adenine dinucleotide by the pyridine nucleotide transhydrogenase of *Escherichia coli*, Biochim. Biophys. Acta 1231 (1995) 297–303.
[24] P.D. Bragg, C. Hou, The role of conserved histidine residues in the pyridine nucleotide transhydrogenase of *Escherichia coli*, Eur. J. Biochem. 241 (1996) 611–618.
[25] P.D. Bragg, C. Hou, Characterisation of mutants of beta-histidine91, beta-aspartate213 and beta-asparagine222, possible components of the energy-transduction pathway of the proton-translocating pyridine nucleotide transhydrogenase of *Escherichia coli*, Arch. Biochem. Biophys. 388 (2001) 299–307.
[26] M. Yamaguchi, C.D. Stout, Y. Hatefi, The proton channel of the energy-transducing nicotinamide nucleotide transhydrogenase of *Escherichia coli*, J. Biol. Chem. 277 (2002) 33670–33675.
[27] S.S. Hasnain, K.O. Hodgson, Structure of metal centres in proteins at subatomic resolution, J. Synchr. Rad. 6 (1999) 852–864.
[28] P.K. Smith, R.I. Krohn, G.T. Hermanson, A.K. Mallia, F.H. Gartner, M.D. Provenzano, E.K. Fujimoto, N.M. Goeke, B.J. Olson, D.C. Klenk, Measurement of protein using bicinchoninic acid, Anal. Biochem. 150 (1985) 76–85.
[29] H. Matsubara, Purification and assay of thermolysin, in: G.E. Perlmann, L. Lorand (Eds.), Proteolytic Enzymes, vol.19 of Methods in Enzymology, Academic Press, 1970, pp. 642–651.
[30] F. D'Acapito, S. Colonna, S. Pascarelli, A. Antonioli, G., Â. Balerna, A. Bazzini, F. Boscherini, G. Campolungo, F., Â. Chini, G. Dalba, G. Davoli, P. Fornasini, R. Graziola, C. Licheri, G., Â. Meneghini, F. Rocca, L. Sangiorgio, V. Sciarra, V. Tullio, S. Mobilio, GILDA (Italian beamline) on BM8, ESRF Newsletters 30 (1998) 42.
[31] S. Pascarelli, F. Boscherini, F. D'Acapito, J. Hardy, C. Meneghini, S. Mobilio, X-ray optics of a dynamical sagittal focussing monochromator on the GILDA beamline at the ESRF, J. Synchr. Rad. 3 (1996) 147–155.
[32] G. Ciatto, F. D'Acapito, F. Boscherini, S. Mobilio, Treatment of EXAFS data taken in fluorescence mode in non-linear conditions, J. Synchr. Rad. 11 (2004) 278–283.
[33] M. Newville, P. Livins, Y. Yacoby, J.J. Rehr, E.A. Stern, Near-edge X-ray-absorption fine structure of Pb: a comparison of theory and experiment, Phys. Rev., B Condens. Matter 47 (1993) 14126–14131.
[34] B. Ravel, M. Newville, ATHENA, ARTEMIS, HEPHAESTUS: data analysis for X-ray absorption spectroscopy using IFEFFIT, J. Synchr. Rad. 12 (2005) 537–541.
[35] J.J. Rehr, R.C. Albers, Theoretical approaches to X-ray absorption fine structure, Rev. Mod. Phys. 72 (2000) 621–654.
[36] P. Ugliengo, D. Viterbo, G. Chiari, MOLDRAW: molecular graphics on a personal computer, Z. Kristallogr. 207 (1993) 9.
[37] M.M. Harding, Small revisions to predicted distances around metal sites in proteins, Acta Crystallogr., D Biol. Crystallogr. 62 (2006) 678–682.
[38] R. Engh, R. Huber, Accurate bond and angle parameters for X-ray protein structure refinement, Acta Cryst. A 47 (1991) 392–400.
[39] N. Dimakis, G. Bunker, XAFS Debye–Waller factors for Zn metalloproteins, Phys. Rev. B 70 (2004) 195114.
[40] N. Binsted, R.W. Strange, S.S. Hasnain, Constrained and restrained refinement in EXAFS data analysis with curved wave theory, Biochemistry 31 (1992) 12117–12125.
[41] Y. Joly, X-ray absorption near-edge structure calculations beyond the muffin-tin approximation, Phys. Rev. B 63 (2001) 125120.
[42] L. Giachini, G. Veronesi, F. Francia, G. Venturoli, F. Boscherini, Synergic approach to XAFS analysis for the identification of most probable binding motifs for mononuclear zinc sites in metalloproteins, J. Synchrotron. Radiat. 17 (2010), doi:10.1107/S090904950904919X.
[43] M.C. Feiters, A.P.A.M. Eijkelenboom, H.-F. Nolting, B. Krebs, F.M.I. van den Ent, R.H.A. Plasterk, R. Kaptein, R. Boelens, X-ray absorption spectroscopic studies of zinc in the N-terminal domain of hiv-2 integrase and model compounds, J. Synchr. Rad. 10 (2003) 86–95.
[44] K. Clark-Baldwin, D.L. Tierney, N. Govindaswamy, E.S. Gruff, C. Kim, J. Berg, S.A. Koch, J.E. Penner-Hahn, The limitations of X-ray absorption spectroscopy for determining the structure of zinc sites in proteins. When is a tetrathiolate not a tetrathiolate? J. Am. Chem. Soc. 120 (1998) 8401–8409.
[45] I.L. Alberts, K. Nadassy, S.J. Wodak, Analysis of zinc binding sites in protein crystal structures, Protein Sci. 7 (1998) 1700–1716.
[46] K.-C. Cheung, R.W. Strange, S.S. Hasnain, 3d EXAFS refinement of the Cu site of azurin sheds light on the nature of structural change at the metal centre in an oxidation–reduction process: an integrated approach combining EXAFS and crystallography, Acta Crystallogr. D 56 (2000) 697–704.
[47] M.A. Holmes, B.W. Matthews, Structure of thermolysin refined at 1.6 A resolution, J. Mol. Biol. 160 (1982) 623–639.
[48] L.M. Murphy, R.W. Strange, S. Hasnain, A critical assessment of the evidence from XAFS and crystallography for the breakage of the imidazolate bridge during catalysis in CuZn superoxide dismutase, Structure 5 (1997) 371–379.
[49] L. Giachini, F. Francia, L. Cordone, F. Boscherini, G. Venturoli, Cytochrome *c* in a dry trehalose matrix: structural and dynamical effects probed by X-ray absorption spectroscopy, Biophys. J. 92 (2007) 1350–1360.
[50] J. Meuller, J. Rydstrom, The membrane topology of proton-pumping *Escherichia coli* transhydrogenase determined by cysteine labelling, J. Biol. Chem. 274 (1999) 19072–19080.